AD-A181 047 SECONDARY RADIATION-DRIVEN THERMAL INSTABILITY(U) NAVAL 1/1
RESEARCH LAB WASHINGTON DC L P GOLDBERG ET AL.
04 MAY 87 NRL-MR-5964

UNCLASSIFIED F/G 3/2 NL

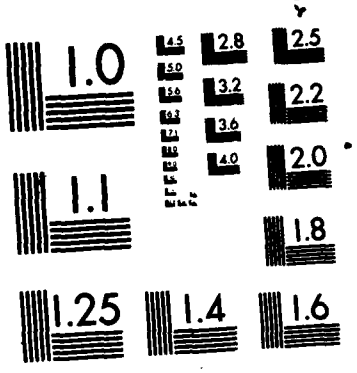

Naval Research Laboratory
Washington, DC 20375-5000

NRL Memorandum Report 5964

Secondary Radiation-Driven Thermal Instability

L. P. GOLDBERG

Department of Physical Sciences
Glassboro State College
Glassboro, NJ 08028

R. B. DAHLBURG

Laboratory for Computational Physics

May 4, 1987

Approved for public release; distribution unlimited.

SECURITY CLASSIFICATION OF THIS PAGE

REPORT DOCUMENTATION PAGE

1a. REPORT SECURITY CLASSIFICATION UNCLASSIFIED	1b RESTRICTIVE MARKINGS
2a. SECURITY CLASSIFICATION AUTHORITY	3. DISTRIBUTION/AVAILABILITY OF REPORT Approved for public release; distribution unlimited.
2b. DECLASSIFICATION/DOWNGRADING SCHEDULE	
4. PERFORMING ORGANIZATION REPORT NUMBER(S) NRL Memorandum Report 5964	5. MONITORING ORGANIZATION REPORT NUMBER(S)
6a. NAME OF PERFORMING ORGANIZATION Naval Research Laboratory 6b. OFFICE SYMBOL (If applicable) Code 4440	7a. NAME OF MONITORING ORGANIZATION
6c. ADDRESS (City, State, and ZIP Code) Washington, DC 20375-5000	7b. ADDRESS (City, State, and ZIP Code)
8a. NAME OF FUNDING/SPONSORING ORGANIZATION Office of Naval Research 8b. OFFICE SYMBOL (If applicable)	9 PROCUREMENT INSTRUMENT IDENTIFICATION NUMBER
8c. ADDRESS (City, State, and ZIP Code) Arlington, VA 22217	10. SOURCE OF FUNDING NUMBERS PROGRAM ELEMENT NO. 61153N; PROJECT NO. RR011-09-43; TASK NO; WORK UNIT ACCESSION NO. DN280-069
11. TITLE (Include Security Classification) Secondary Radiation-Driven Thermal Instability	
12. PERSONAL AUTHOR(S) Goldberg, L. P. and Dahlburg, R. B.	
13a. TYPE OF REPORT 13b TIME COVERED FROM _____ TO _____ 14 DATE OF REPORT (Year, Month, Day) 1987 May 4 15 PAGE COUNT 30	
16. SUPPLEMENTARY NOTATION	
17. COSATI CODES FIELD / GROUP / SUB-GROUP	18 SUBJECT TERMS (Continue on reverse if necessary and identify by block number) Instability; Condensation; Solar atmosphere.

19. ABSTRACT (Continue on reverse if necessary and identify by block number)

We determine by means of numerical simulation the two-dimensional stability properties of the one-dimensional secondary equilibrium state of a radiation-driven thermally unstable fluid reported by Oran, Mariska, and Boris (1982). We find that strong secondary instabilities occur, and that the perturbed system tends to move toward a two-dimensional state. The mass density forms clump-like structures, while the temperature profile exhibits a kink-like instability. In an appendix we formulate an eigenvalue problem for the linear stability of the secondary equilibrium.

20 DISTRIBUTION/AVAILABILITY OF ABSTRACT ☒ UNCLASSIFIED/UNLIMITED ☐ SAME AS RPT ☐ DTIC USERS	21 ABSTRACT SECURITY CLASSIFICATION UNCLASSIFIED
22a NAME OF RESPONSIBLE INDIVIDUAL R. B. Dahlburg	22b TELEPHONE (Include Area Code) (202) 767-3055 22c OFFICE SYMBOL Code 4440

DD FORM 1473, 84 MAR 83 APR edition may be used until exhausted
All other editions are obsolete

SECURITY CLASSIFICATION OF THIS PAGE

GPO U.S. Government Printing Office: 1985—607-047

CONTENTS

SECONDARY RADIATION-DRIVEN THERMAL INSTABILITY

I. INTRODUCTION

Oran, Mariska, and Boris (1982) investigated the stability of a one-dimensional plasma at temperatures and densities typical of the solar transition region and corona, using both a linear analysis and non-linear time-dependent numerical simulations. Under constant pressure conditions with a steady heat source H, some regions of a plasma cool while other regions are heated. The rate at which this process occurs depends on the balance of H and the radiative loss rate S. The radiation loss rate of a plasma, S, varies in a complex way with the mass density and temperature. When S increases faster with the mass density than it decreases with a lowering of the temperature, the cooling regions will tend to condense as the plasma attempts to maintain pressure balance. This phenomenon is termed the condensational instability. On the other hand, the hotter regions will expand and tend to grow hotter as the steady heating (per unit volume) becomes dominant over the radiation cooling process. This runaway temperature effect is usually called the radiation-driven thermal instability (Priest 1982). We will use this latter designation to refer to either process.

Oran, Mariska and Boris started from an isotropic static equilibrium state. They perturbed this state with single mode disturbances in the velocity field, and observed that the plasma condensed into one or more cool dense regions with a hot tenuous surrounding. The condensations appeared to reach a secondary equilibrium.

Manuscript approved January 21, 1987.

but they emphasized that they had performed only one-dimensional simulations and questioned whether their final state might be unstable in two or three dimensions.

We report here on preliminary results of an investigation into the radiation-driven thermal instability of a one-dimensional secondary equilibrium. Starting from a one-dimensional secondary equilibrium state, we have performed a series of non-linear simulations in two-dimensions and found that the secondary equilibrium is indeed unstable to random two-dimensional perturbations.

In § II we describe the governing equations and numerical method. The computational procedure, which is based on the FAST2D hydrodynamic algorithm, is the same as that employed by Dahlburg, *et al.* (1987). In § III we describe the one-dimensional simulation performed to obtain the secondary equilibrium state. We augment the description of this system given by Oran, Mariska and Boris (1982) by describing the energetics of the system. In § IV the results of the two-dimensional runs are described. We typically see the system move rapidly away from the one-dimensional secondary equilibrium state. In § V we discuss the results in the context of the upper solar atmosphere. In the appendix we formulate an eigenvalue problem for infinitesimal disturbances of the secondary equilibrium.

II. FORMULATION OF THE PROBLEM

We consider a compressible, two-dimensional, uniform, fluid medium in Cartesian geometry (see Field 1965, § II). The evolution of this fluid is governed by the equations of continuity, motion, energy, and state, which are written below in conservation form:

$$\frac{\partial \rho}{\partial t} + \nabla \cdot (\rho \mathbf{v}) = 0 , \tag{1a}$$

$$\frac{\partial \rho \mathbf{v}}{\partial t} + \nabla \cdot (\rho \mathbf{v}\mathbf{v}) = -\nabla P , \tag{1b}$$

$$\frac{\partial E}{\partial t} + \nabla \cdot \Big[(E + P)\mathbf{v}\Big] = \nabla \cdot (\kappa \nabla T) + H - S(\rho, T), \tag{1c}$$

$$P = (\gamma - 1)U, \tag{1d}$$

where: $\rho(x, y, t)$ = mass density, $\mathbf{v}(x, y, t) = (u, v, 0)$ = flow velocity, $U(x, y, t)$ = internal energy density, $E(x, y, t)$ = total energy density = $U(x, y, t) + \frac{1}{2}\rho|\mathbf{v}|^2$, $P(x, y, t)$ = mechanical pressure, $T(x, y, t)$ = thermodynamic temperature, $\kappa(\rho, T)$ = thermal conductivity tensor, H = heating rate, $S(\rho, T)$ = radiative loss function, and γ = ratio of specific heats = 5/3 for an ideal monatomic gas. For the radiative loss function, $S(\rho, T)$, we use the model employed by Oran, Mariska, and Boris (1982). Periodic boundary conditions are imposed in both spatial directions.

The primary equilibrium state for the system of equations 1a - 1d is given by: $\rho = \rho_0$ = constant, $\mathbf{v} = 0$, $U = U_0$ = constant, and $H = S(\rho_0, T_0)$ = constant. In this report, we use the same values for these constants as Dahlburg, *et al.*, *viz.*, (1986) $\rho_0 = 3.07 \times 10^{-14}$ g cm^{-3}, $U_0 = 4.85$ erg cm^{-3}, $H_0 = 0.0272$ erg cm^{-3} s^{-1}, $\kappa = 1.14 \times 10^{-6}\, T^{2.5}$ erg cm^{-1} s^{-1} K^{-1}, and $T_0 = 7.29 \times 10^5$ K. We use this static equilibrium state to initialize our one-dimensional code.We then perturb this state and evolve the system in time until a state of secondary equilibrium is achieved.

The numerical method used to solve equations 1a - 1d is described in detail by Dahlburg *et al.* (1987). Here we give a brief description of the algorithm. Centered differences are used to discretize both spatial directions. For the two-dimensional simulations reported in this paper, the system is a square region 9.19×10^8 cm on edge. This size represents one wavelength of the characteristic perturbation used by Oran, Mariska, and Boris (1982) for the temperature and mass conditions under study. The region is divided into a 100 by 100 grid with uniformly spaced intervals of 9.19×10^6 cm. A time-step splitting scheme is used which separates

the hydrodynamic processes from the thermodynamic processes. The hydrodynamic terms are advanced in time by the flux-corrected transport method, with a predictor-corrector method employed to time-center the source terms. For time advancing the thermodynamic terms, an iterative alternating direction implicit scheme is used.

III. ONE-DIMENSIONAL RESULTS

In this section we describe the results of the one-dimensional run performed to obtain the secondary equilibrium state. To run the two-dimensional code in this one-dimensional mode we use 4 uniform cells in the y direction, with $\Delta y = \Delta x$. No variation in y is permitted. We perturb the static equilibrium state described in § II with random perturbations in the x-velocity component and allow the system to evolve in time, where the system length is given by $L_x = 9.19 \times 10^8$ cm. We terminate the run when we are satisfied that a state of secondary equilibrium has been achieved, *i.e.*, when the system has stabilized at a different state. Our simulation differs from that of Oran, Mariska, and Boris in two respects. First, we use periodic boundary conditions. Second, we use random initial conditions in the velocity field so that the system can traverse as wide a range of phase space as possible. Although our simulation differs in some respects from those of Oran, Mariska, and Boris (1982), our results appear to confirm theirs.

The evolution of the system as a whole is represented by the internal energy. Figure 1 shows the internal energy, $\int_0^{L_x} U\,dx$, as a function of time. This, and all subsequent global quantities, is defined per unit length in the z direction. The internal energy remains approximately constant, near the primary equilibrium value, as long as the perturbations remain small. When the perturbations attain finite amplitude, as evidenced by the rapid growth in the kinetic energy, the internal energy drops precipitously. Some growth due to reheating is seen, and then the internal energy remains approximately constant for approximately 900 seconds. We regard this constant behaviour of the global quantities as sufficient evidence that the system

has attained a state of secondary equilibrium. Further evidence that a secondary equilibrium state has been achieved is shown in figure 2, which shows the energy deficit, $E_d = \int_0^{L_x} \int_0^{t_s} [S(\rho, T) - H]\, dx\, dt$, as a function of time. The energy deficit remains approximately constant for almost 700 s, showing that the heat energy input and the radiation enrgy losses are about equal in the vicinity of the primary equilibrium. This equilibrium is destroyed by the formation of condensates, which are extremely effective radiators during their formation phase. After some time a state of secondary equilibrium is achieved in which the spatially varying radiation energy losses equal the heat energy input. The maintenance of this equilibrium depends on thermal conduction and convection for the transport of heat energy to those locations which are radiating energy most efficiently.

Figure 3 shows the mass density profile, $\rho(x)$ at secondary equilibrium. Figure 4 shows the corresponding temperature profile $T(x)$. We see that after saturation, a cool, dense region is able to exist in equilibrium with a hot, rare region. The maximum mass density in the condensed region is 4.5×10^{-12} g cm^{-3}, at a temperature of 4.2×10^4 K. The minimum mass density in the rarefied region is 1.1×10^{-13} g cm^{-3}, at a temperature of 1.7×10^6 K.

IV. TWO-DIMENSIONAL RESULTS

In this section we determine numerically whether the one-dimensional equilibrium state described in § III is subject in two-dimensions to secondary radiation-driven thermal instabilities. We choose $L_y = L_x$.

We here describe one run which is representative of those which we performed in detail. Figure 5 is a vector plot of the initial velocity field perturbation. To avoid cluttering the plot, the velocity field is represented on a reduced set of points. The perturbed velocity field is determined by the method used by Dahlburg, *et al.* (1987). Figure 6 shows the kinetic energy, $\frac{1}{2} \int_0^{L_x} \int_0^{L_y} \rho \mid \mathbf{v} \mid^2 dx\, dy$, as a function of time. Starting from an initial value of about 5.2×10^{16} ergs there is at first a

very rapid drop. Then after a slight rise, the kinetic energy drops for a period of about 500 s as it flows into other forms of energy available to the system. The rate of decay decreases steadily and the kinetic energy appears to approach a limiting value of about 1.1×10^{16} ergs.

Figure 7 shows the internal energy, $\int_0^{L_x} \int_0^{L_y} U \, dx \, dy$, as a function of time. Starting from as initial value of about 3.45×10^{18} ergs, this is seen to decrease at an almost constant rate for about 180 s. Subsequently, the rate of decay decreases. At the end of the simulation, t = 727 s, the internal energy is equal to 2.2×10^{18} ergs.

Figure 8 shows the energy deficit, $E_d = \int_0^{L_x} \int_0^{L_y} \int_0^{t_e} \left[S(\rho, T) - H\right] dx \, dy \, dt$, as a function of time. This represents the radiation energy reduced by the amount of heating energy. Initially this quantity is zero, representing the thermodynamic equilibrium of radiation energy losses and constant heat energy input. It rises steadily from zero at a rapid rate for about 180 s. After this time, the rate of increase appears to decline. At the final time the energy deficit is equal to 1.3×10^{18} ergs. The rate of increase of the energy deficit is consistent with the rate of decrease of the internal energy. This suggests that radiation is produced mainly at the expense of the internal energy, and that the kinetic energy is maintained by the heating source. This also suggests that the most prominent effect produced by the perturbing of the system is the production of more radiated energy.

Figure 9 is a contour plot of the mass density at the final time. It shows considerable concentration of mass in 2 regions of the plot. The mass density appears to be kinking, with high density regions forming at the extremities of the kink. The maximum mass density is about 8.6×10^{-13} g cm^{-3}, while the minimum value is 6.2×10^{-15} g cm^{-3}. These values differ by a factor of about 140. Figure 10 is a contour plot of the temperature at the same time. The kinking is also apparent in the temperature field, but it appears to retain the bifurcated character of the secondary equilibrium. The maximum temperature is about 1.6×10^6 K, while the

minimum value is 1.2×10^4 K. These values differ by about the same amount as the mass density maximum and minimum. Figure 11 is a vector plot of the final velocity field. A very active flow region is visible at the lower right. The twisting action implies high vorticity, which should promote the formation of a two-dimensional state. Figure 12 is a contour plot of the dilation factor, or divergence, of the fluid. A positive dilation factor signifies fluid rarefaction, and a negative dilation factor signifies fluid compression. This figure shows that a rarefaction zone develops ahead of the high mass density regions, while a condensing region forms behind this zone.

When very large amplitude perturbations were attempted, say with 25 times the energy of those described, the time-step, which is adjusted for each step of the simulation in response to the hydrodynamic and thermal conduction time scales (see Dahlburg *et al.* 1987), became so small that even after 5000 steps of the simulation the total elapsed time was less than half a second. Presumably in this case the high characteristic velocity produced results in an extremely short hydrodynamic time scale.

V. DISCUSSION

In this investigation we have seen the radiation-driven thermally unstable fluid exhibit a tendency to move away from a one-dimensional state toward a two-dimensional state. In the absence of any restoring force, it is clear that the fluid will not return to its initial state. Unfortunately, due to the high cost of these numerical simulations we were not able to extend our calculations farther in time and so determine the long-time state of the fluid. The high cost results from the severe time-step restriction imposed by the thermal conduction time-scale. We conjecture that eventually the sheet will break up.

Analysis of this phenomenon is difficult due to the high order and extreme nonlinearity of the governing system of partial differential equations. In the appendix

we take a first step in analysis by formulating an eigenvalue problem for the linear stability of the secondary equilibrium.

In practice it is difficult to observe the evolution of un. table fluids in the solar corona and transition region because it has not been possible yet to achieve the necessary spatial and temporal resolution in the observing instruments. Recently, faint superspicules were reported by Breuckner *et al.* (1986). These superspicules were seen on the disk of the sun close to the limb, and they appeared to form in space rather than to have been ejected upward from the surface. Their available temporal resolution, at best 20 s, but generally about 60 s, would not permit Breuckner *et al.* to observe the evolution of this short-lived phenomenon (as little as 180 s). They did see the superspicules flex and bend in the course of their development. These superspicules could conceivably condense out of the corona as a result of some velocity perturbation arising from the turbulent nature of the surrounding medium. Since the corona is very tenuous, the amount of mass and consequently the intensity of the radiation from these condensations would be quite small. This would explain their very faint nature.

Zirin (1966) has stated that "loops and coronal rain typically occur as the aftermath of flares and surges". It is not inconceivable that these phenomena also could arise from the velocity perturbations produced by flares which then produce condensations observed as loops and coronal rain.

The work performed here can be extended by changing the initial conditions, or the magnitude of the perturbations, or simply by adding the force of gravity into the calculation to see the effect on the results. A more difficult extension would be to include the effects of magnetic fields to simulate more realistically the magnetofluids in the transition region and corona of the sun. Potentially, this program might be applied to a variety of phenomena in the sun or elsewhere in the universe to aid in the interpretation of the various phenomena which are observed (see Field 1965).

ACKNOWLEDGEMENTS

We thank Dr. J. T. Karpen and Dr. J. M. Picone for helping to acquire the one-dimensional results. This work was performed while L. P. G. was a faculty participant at the Naval Research Laboratory under the American Society for Engineering Education Summer Faculty Program. R. B. D. was sponsored by the National Aeronautics and Space Administration Solar Terrestrial Theory Program and by the Office of Naval Research. The numerical simulations reported here were partially supported by a generous grant of computer time on the NRL CRAY-XMP from the director of research of the Naval Research Laboratory.

REFERENCES

Breuckner, G. E., Bartoe, J. -D. F., Cook, J. W., Dere, K. P., and Socker, D. G., *Presentation Release*: "HRTS Results from Spacelab 2". 1986, *Ap. J.*, **142**, 531.

Dahlburg, R. B., DeVore, C. R., Picone, J. M., Mariska, J. T., and Karpen, J. T., 1987, *Ap. J.*, in press.

Field, G. B. 1965, *Ap. J.*, **142**, 531.

Oran, E. S., Mariska, J. T., and Boris, J. P. 1982, *Ap. J.*, **254**, 349.

Priest, E. R. 1982 *Solar Magnetohydrodynamics*, ((Dordrecht: Reidel).

Zirin, H. 1966, *The Solar Atmosphere*, (Waltham: Ginn Blaisdell).

APPENDIX

In this appendix we derive a generalized eigenvalue problem which determines the linear stability properties of the nonuniform, secondary equilibrium. We first rewrite the governing equations $1a - 1c$, with the pressure eliminated by means of the equation of state $1d$:

$$\frac{\partial \rho}{\partial t} + \nabla \cdot \mathbf{\Psi} = 0\,, \tag{A1a}$$

$$\frac{\partial \mathbf{\Psi}}{\partial t} + \nabla \cdot (\mathbf{\Psi}\mathbf{v}) = -(\gamma - 1)\nabla U\,, \tag{A1b}$$

$$\frac{\partial U}{\partial t} + \nabla \cdot (U\mathbf{v}) = \kappa_0 \nabla \cdot \left(T^{\frac{5}{2}} \nabla T\right) + H - \rho\xi(\rho, T)\,. \tag{A1c}$$

In this formulation we time advance the internal energy, rather than the total energy. The variable Ψ is the momentum, $\rho\mathbf{v}$, and $\xi(\rho, T) \equiv \frac{S(\rho,T)}{\rho}$.

We first linearize equations $A1a - A1c$ about the secondary equilibrium, *i.e.*, we allow the field variables to vary as:

$$\rho = \rho_0(y) + \rho_1(x, y, t)\,, \tag{A2a}$$

$$\mathbf{v} = \mathbf{v}_1(x, y, t)\,, \tag{A2b}$$

$$\mathbf{\Psi} = \mathbf{\Psi}_1(x, y, t)\,, \tag{A2c}$$

$$U = U_0(y) + U_1(x,y,t)\,, \tag{A2d}$$

$$T = T_0(y) + T_1(x,y,t)\,, \tag{A2e}$$

where the subscript 0 indicates the secondary equilibrium field values, and the subscript 1 indicates the perturbed field values.

Substituting equations $A2$ into equations $A1$ and ignoring terms which are quadratic in the perturbed quantities, we have to first order:

$$\frac{\partial \rho_1}{\partial t} + \nabla \cdot \mathbf{\Psi}_1 = 0\,, \tag{A3a}$$

$$\frac{\partial \mathbf{\Psi}}{\partial t} = -(\gamma - 1)\nabla U_1\,, \tag{A3b}$$

$$\frac{\partial U_1}{\partial t} + \nabla \cdot \Big[U_0 \mathbf{v}_1\Big] = \kappa_0 \nabla \cdot (T_0^{\frac{5}{2}} \nabla T_1) - \rho_0 \Big(\frac{\partial \xi}{\partial \rho}\Big)_T \rho_1 - \rho_0 \Big(\frac{\partial \xi}{\partial T}\Big)_\rho \Big(\frac{T_0}{U_0} U_1 - \frac{T_0}{\rho_0}\rho_1\Big) \tag{A3c}$$

The quantities $\left(\frac{\partial \xi}{\partial \rho}\right)_T$ and $\left(\frac{\partial \xi}{\partial T}\right)_\rho$ are evaluated for the equilibrium state. The perturbed temperature, T_1, has been eliminated by the first order equation of state in the radiation loss term. We have not evaluated T_1 in the thermal conduction term for notational simplification.

After some more algebra:

$$\frac{\partial \rho}{\partial t} = -\frac{\partial \Psi_x}{\partial x} - \frac{\partial \Psi_y}{\partial y}\,, \tag{A4a}$$

$$\frac{\partial \Psi_x}{\partial t} = -(\gamma - 1)\frac{\partial U}{\partial x}, \qquad (A4b)$$

$$\frac{\partial \Psi_y}{\partial t} = -(\gamma - 1)\frac{\partial U}{\partial y}, \qquad (A4b)$$

$$\begin{aligned}\frac{\partial U}{\partial t} = &- U_0\Big(\frac{\partial u}{\partial x} + \frac{\partial v}{\partial y}\Big) - \frac{dU_0}{dy}v \\ &+ \kappa_0 \nabla \cdot (T_0^{\frac{5}{2}} \nabla T) - \rho_0\Big(\frac{\partial \xi}{\partial \rho}\Big)_T \rho - \rho_0\Big(\frac{\partial \xi}{\partial T}\Big)_\rho \Big(\frac{T_0}{U_0}U - \frac{T_0}{\rho_0}\rho\Big)\end{aligned} \qquad (A4d)$$

where we have dropped the 1 subscripts. This is a set of linear partial differential equations for infinitesimal disturbances to the secondary equilibrium.

We now perform a normal mode analysis, assuming that the variation of the perturbed quantities is given by:

$$f(x, y, t) = f'(y)e^{i\alpha x - i\omega t}. \qquad (A5)$$

where α is defined to be the x perturbation wavenumber, and ω is the complex growth-rate of the disturbance.

If we define $D \equiv \frac{d}{dy}$, then upon substitution (and ignoring the primed superscripts) we have the following set of ordinary differential equations:

$$-i\omega\rho = -i\alpha\Psi_x - D\Psi_y, \qquad (A6a)$$

$$-i\omega\Psi_x = -i\alpha(\gamma - 1)U, \qquad (A6b)$$

$$-i\omega\Psi_y = -(\gamma-1)DU\,, \tag{A6c}$$

$$-i\omega U = -U_0(i\alpha u + Dv)$$

$$+\kappa_0(DT_0^{\frac{5}{2}})DT + \kappa_0 T_0^{\frac{5}{2}}(D^2T - \alpha^2 T) \tag{A6d}$$

$$-\rho_0\left(\frac{\partial\xi}{\partial\rho}\right)_T\rho - \rho_0\left(\frac{\partial\xi}{\partial T}\right)_\rho\left(\frac{T_0}{U_0}U_1 - \frac{T_0}{\rho_0}\rho_1\right)$$

We have used the the variables Ψ_x, Ψ_y and T to simplify the mathematics. We now eliminate them to reduce the number of variables to the number of equations.

$$i\alpha\rho_0 u + \rho_0 Dv = i\omega\rho\,, \tag{A7a}$$

$$i\alpha(\gamma-1)U = i\omega\rho_0 u\,, \tag{A7b}$$

$$(\gamma-1)DU = i\omega\rho_0 v\,, \tag{A7c}$$

$$\left[\rho_0\left(\frac{\partial\xi}{\partial\rho}\right)_T - \rho_0\left(\frac{\partial\xi}{\partial T}\right)_\rho\left(\frac{T_0}{\rho_0}\right) + \kappa_0\Theta\right]\rho + i\alpha U_0 u + \left[U_0 D - \left(DU_0\right)\right]v$$

$$+\left[\rho_0\left(\frac{\partial\xi}{\partial T}\right)_\rho\left(\frac{T_0}{\rho_0}\right) + \kappa_0\Phi\right]U = i\omega U \tag{A7d}$$

In equation $A7d$ we use the following operators:

$$\Theta = \alpha^2 T_0^{\frac{5}{2}}\zeta_1 - (DT_0^{\frac{5}{2}})\zeta_1 D - (DT_0^{\frac{5}{2}})(D\zeta_1) - T_0^{\frac{5}{2}}\left[(D^2\zeta_1) + 2(D\zeta_1)D + \zeta_1 D^2\right]. \tag{A8a}$$

$$\Phi = -\alpha^2 T_0^{\frac{5}{2}} \zeta_2 + (DT_0^{\frac{5}{2}})\zeta_2 D + (DT_0^{\frac{5}{2}})(D\zeta_2) + T_0^{\frac{5}{2}} \left[(D^2\zeta_2) + 2(D\zeta_2)D + \zeta_2 D^2 \right], \tag{A8b}$$

where $\zeta_1 = \frac{T_0}{\rho_0}$ and $\zeta_2 = \frac{T_0}{U_0}$.

Equations A7 have the form of a generalized eigenvalue problem:

$$\mathbf{A}\mathbf{x} = \omega \mathbf{B}\mathbf{x}. \tag{A9}$$

The eigenvector $\mathbf{x} = (\ \rho\ \ u\ \ v\ \ U\ )^T$, where the superscript T denotes the transpose of the vector $\mathbf{x}$. The eigenvalue is ω, the complex growth rate.

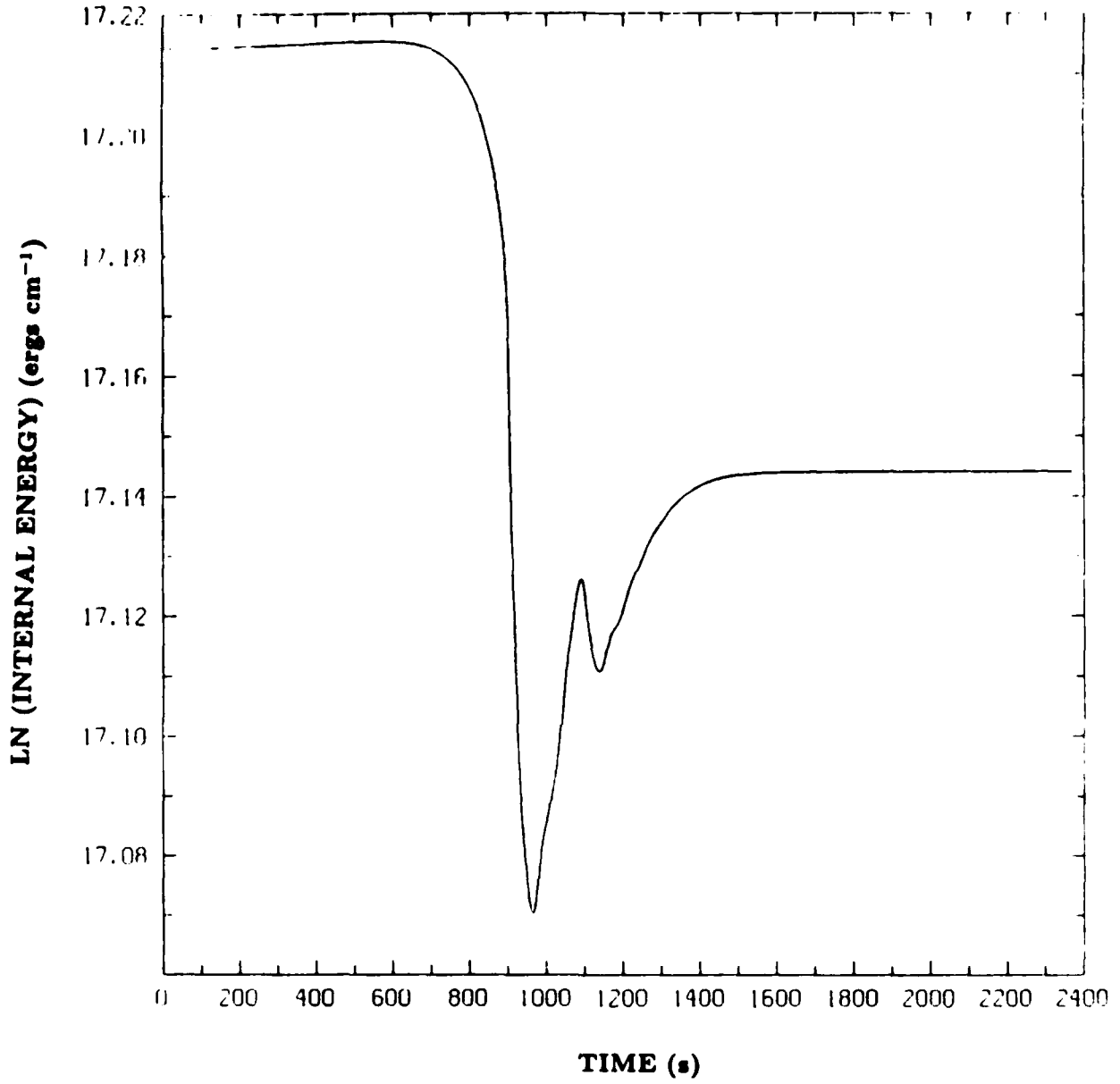

Figure 1. Plot of internal energy *vs* time for one-dimensional simulation.

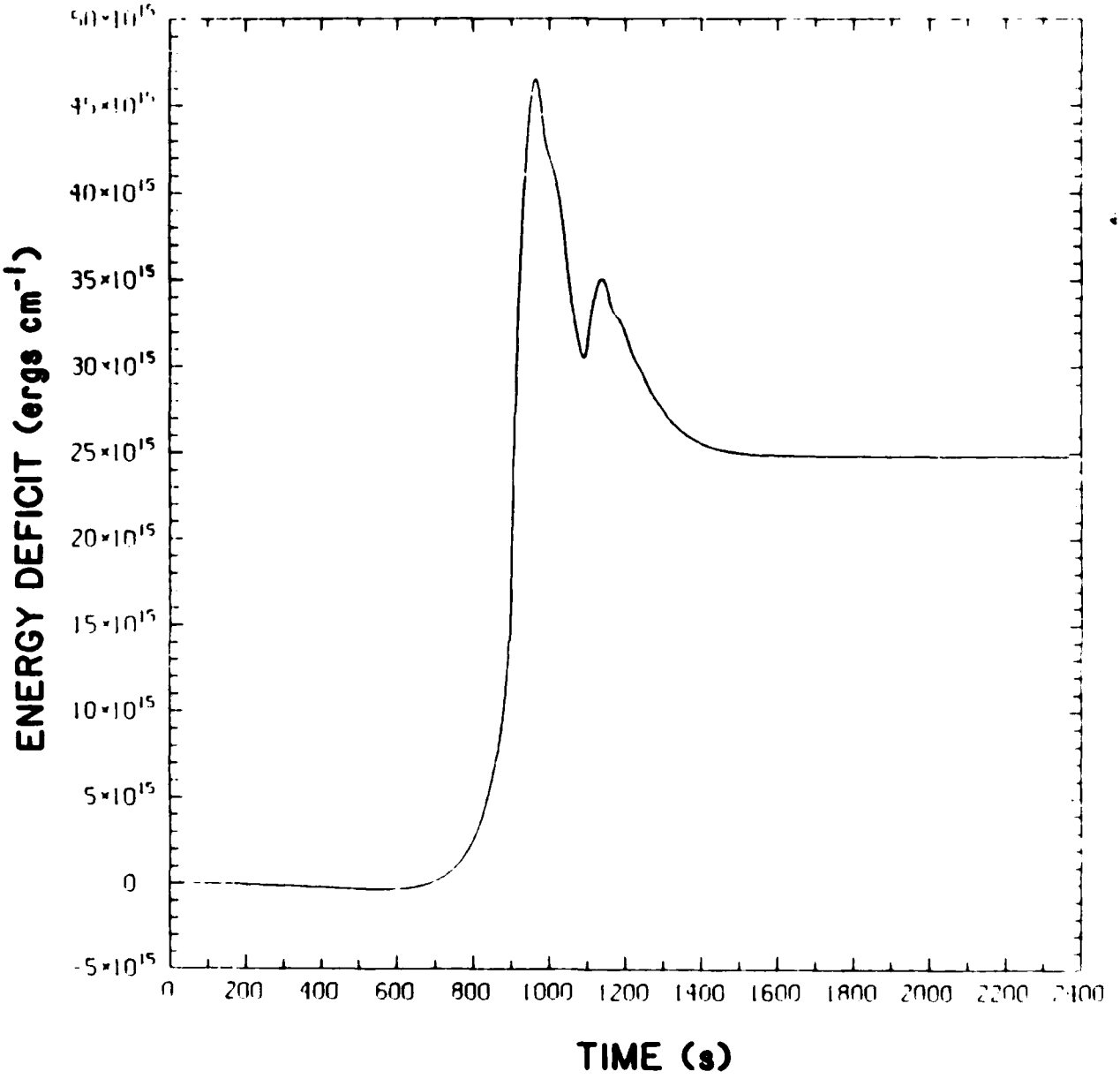

Figure 2. Plot of energy deficit *vs* time for one-dimensional simulation.

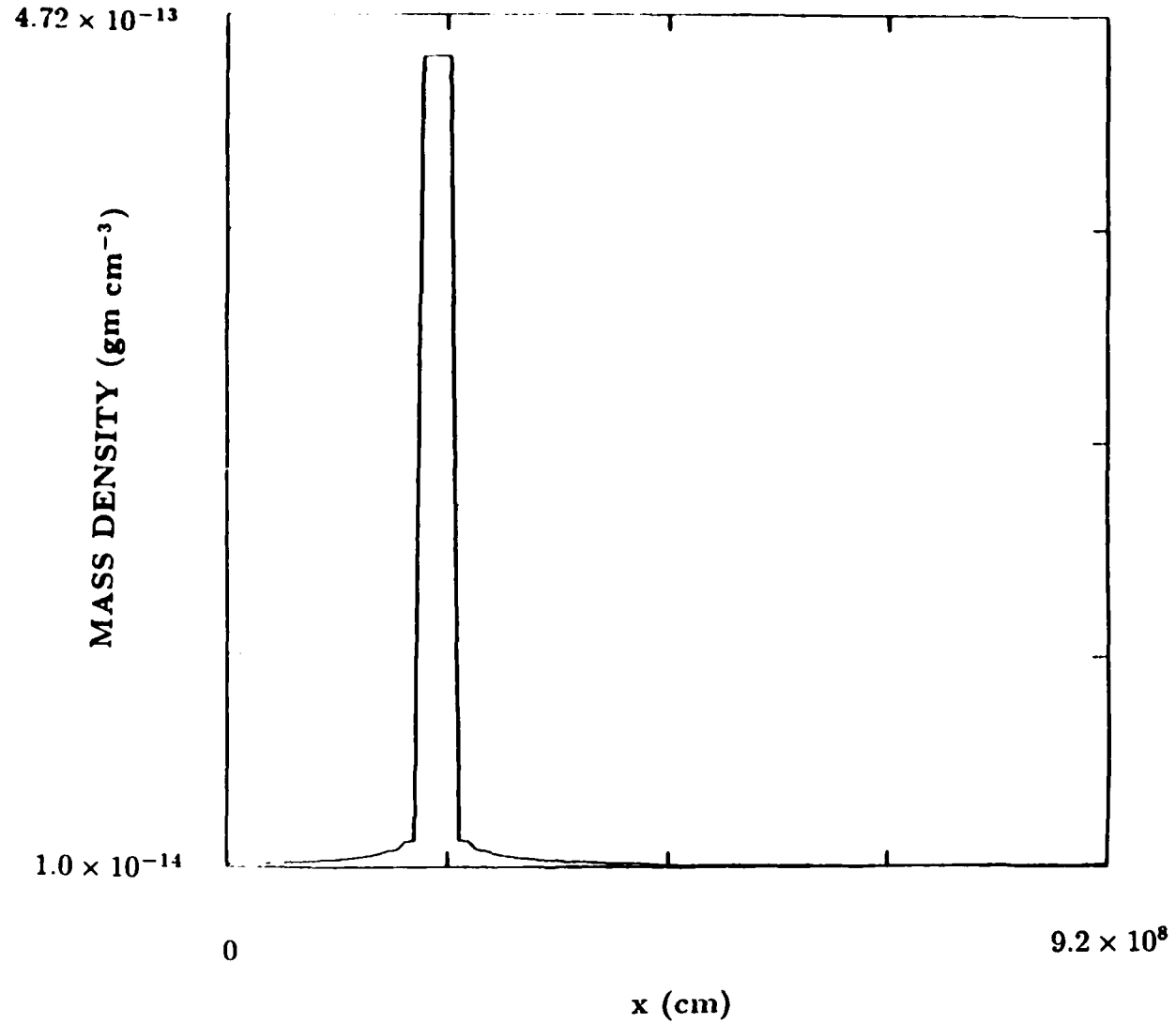

Figure 3. Mass density at secondary equilibrium.

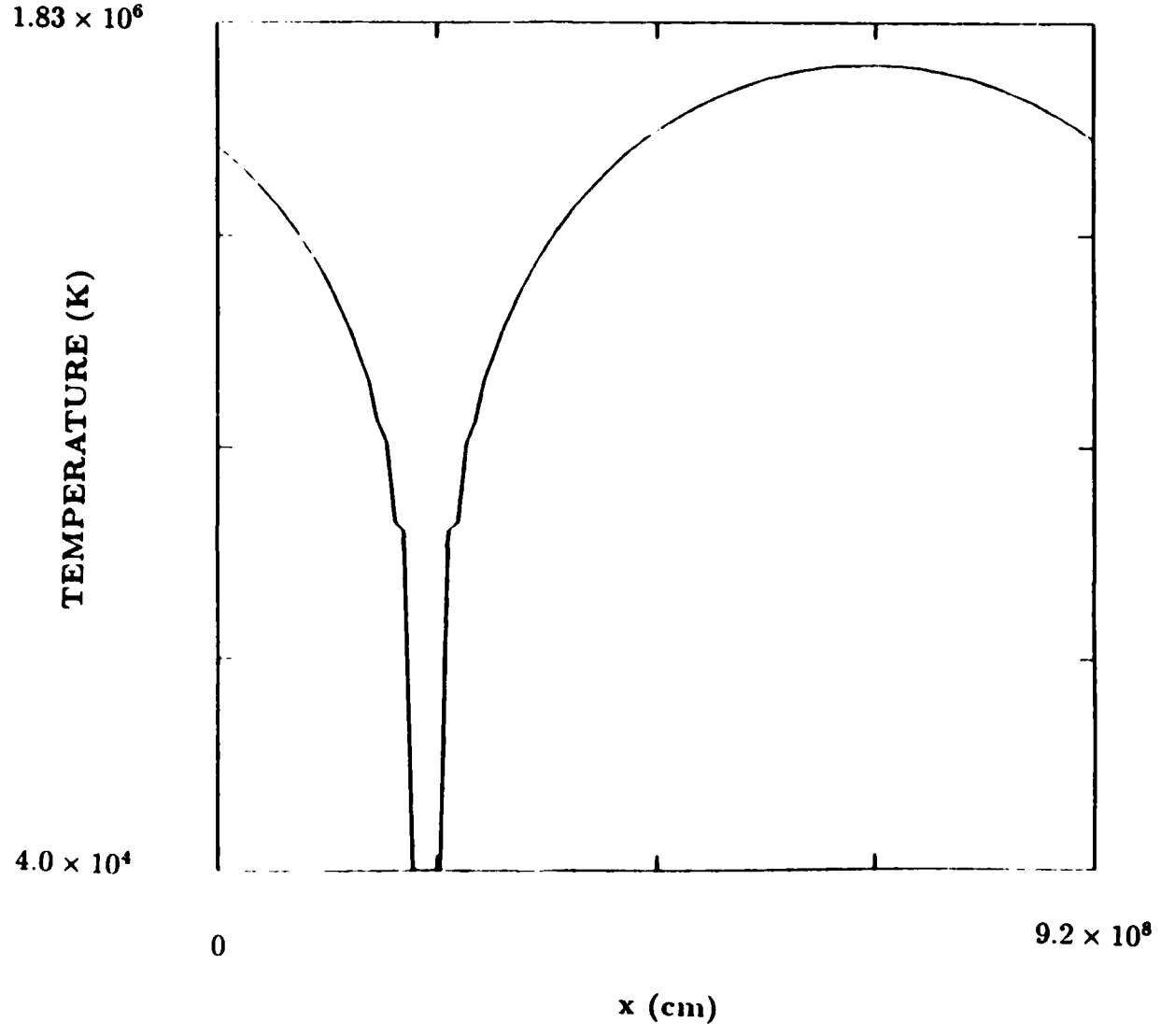

Figure 4. Temperature at secondary equilibrium.

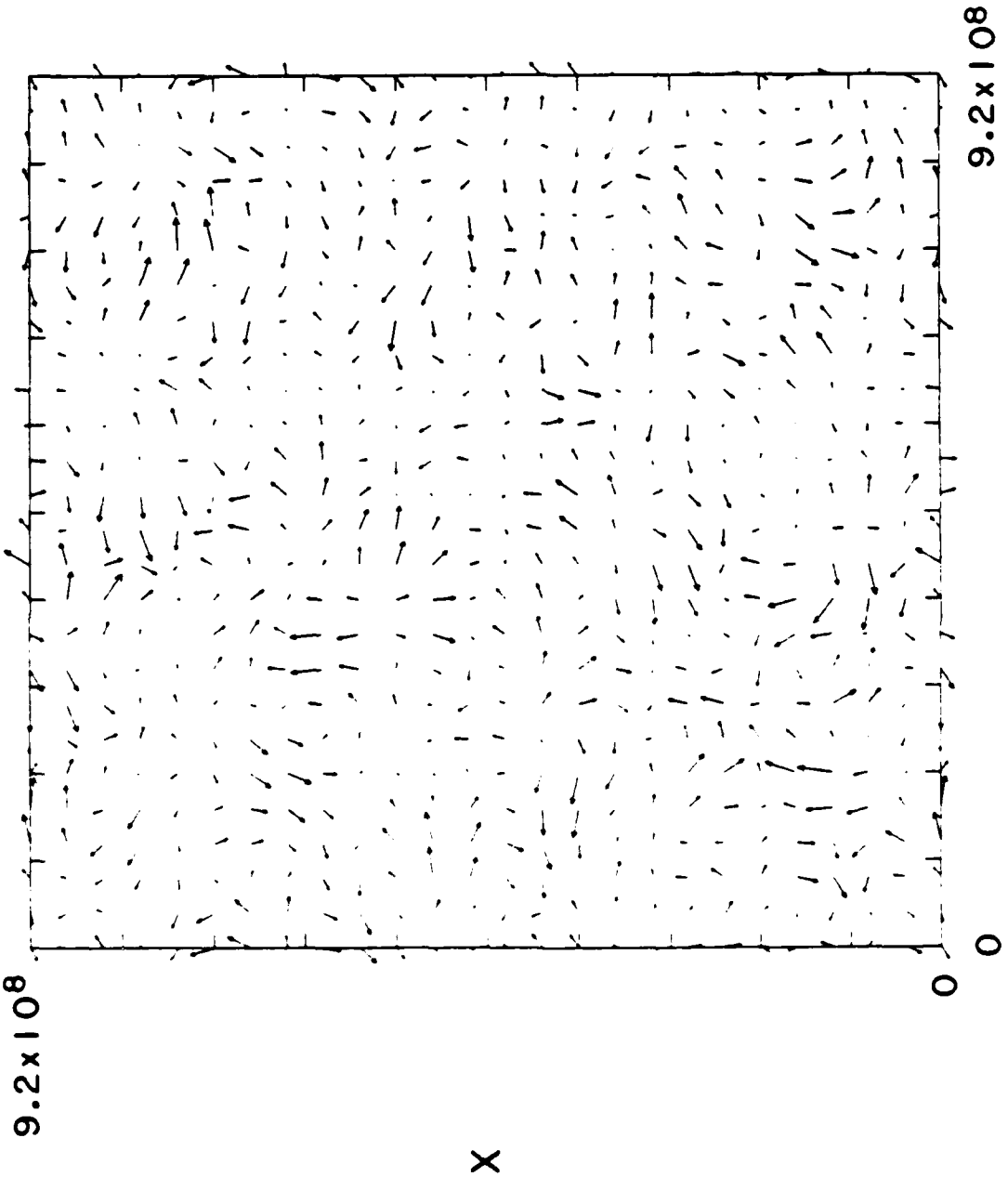

Figure 5. Vector plot of velocity field perturbation for two-dimensional simulation.

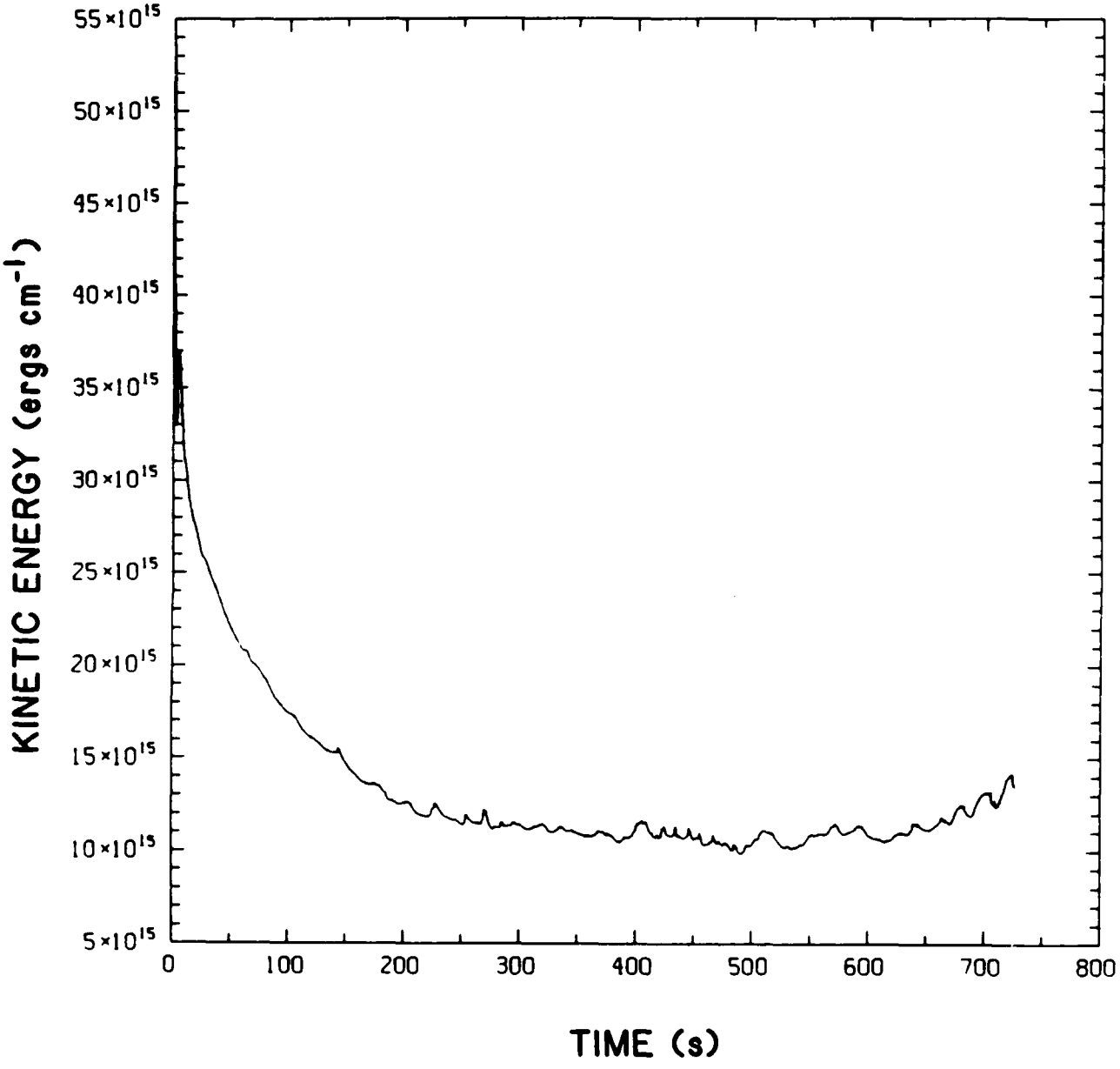

Figure 6. Plot of kinetic energy *vs* time for two-dimensional simulation.

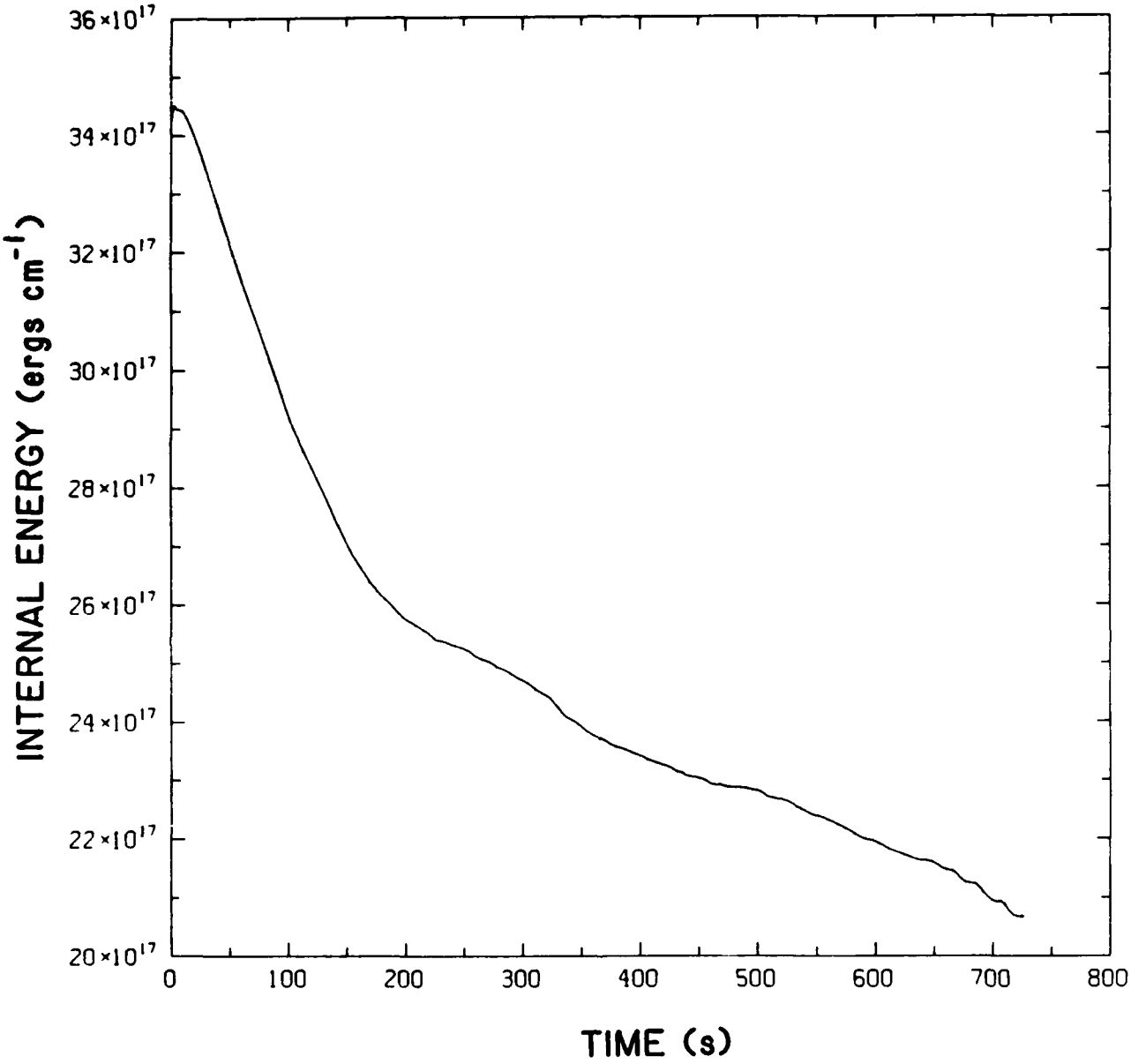

Figure 7. Plot of internal energy *vs* time for two-dimensional simulation.

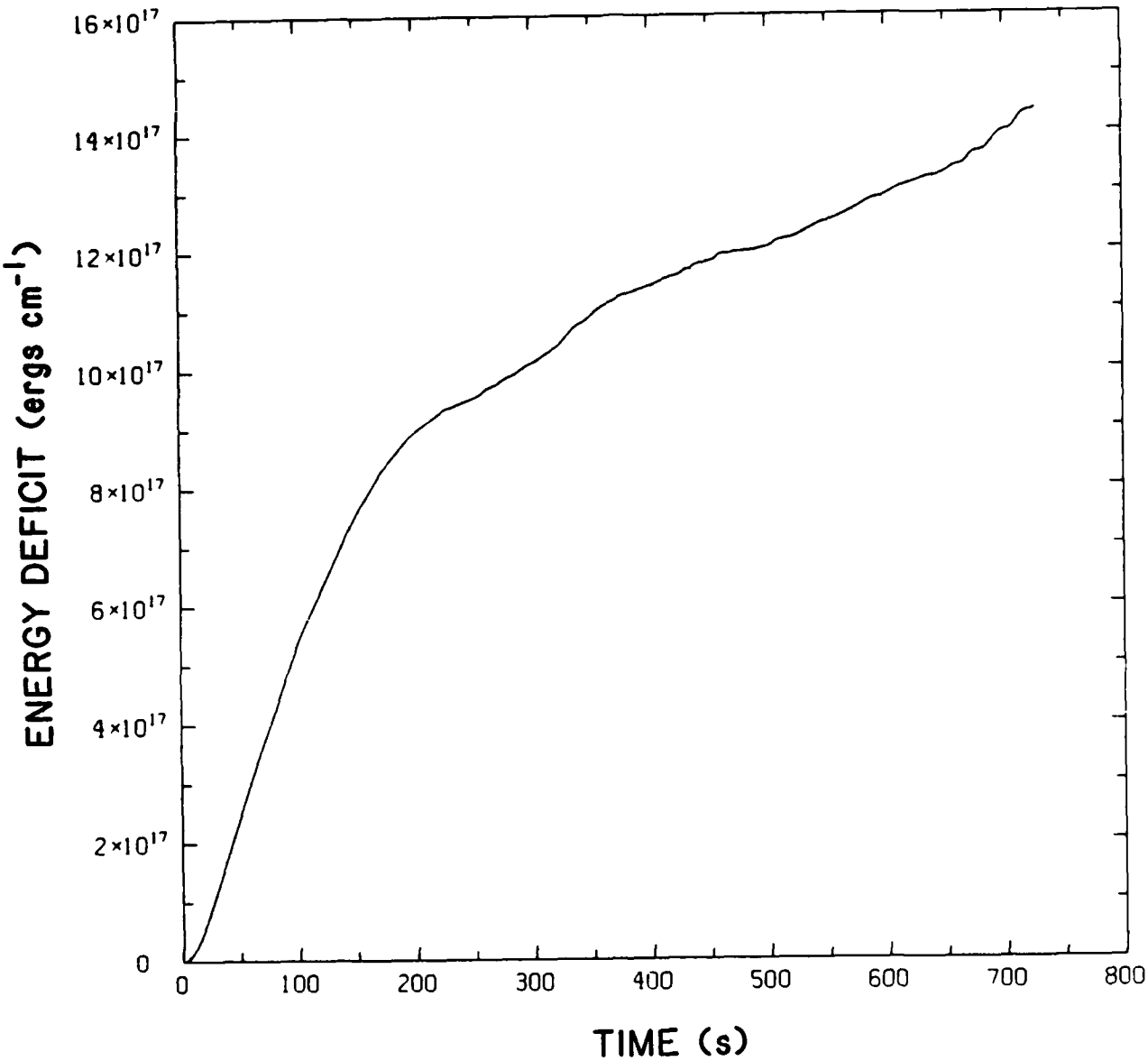

Figure 8. Plot of energy deficit *vs* time for two-dimensional simulation.

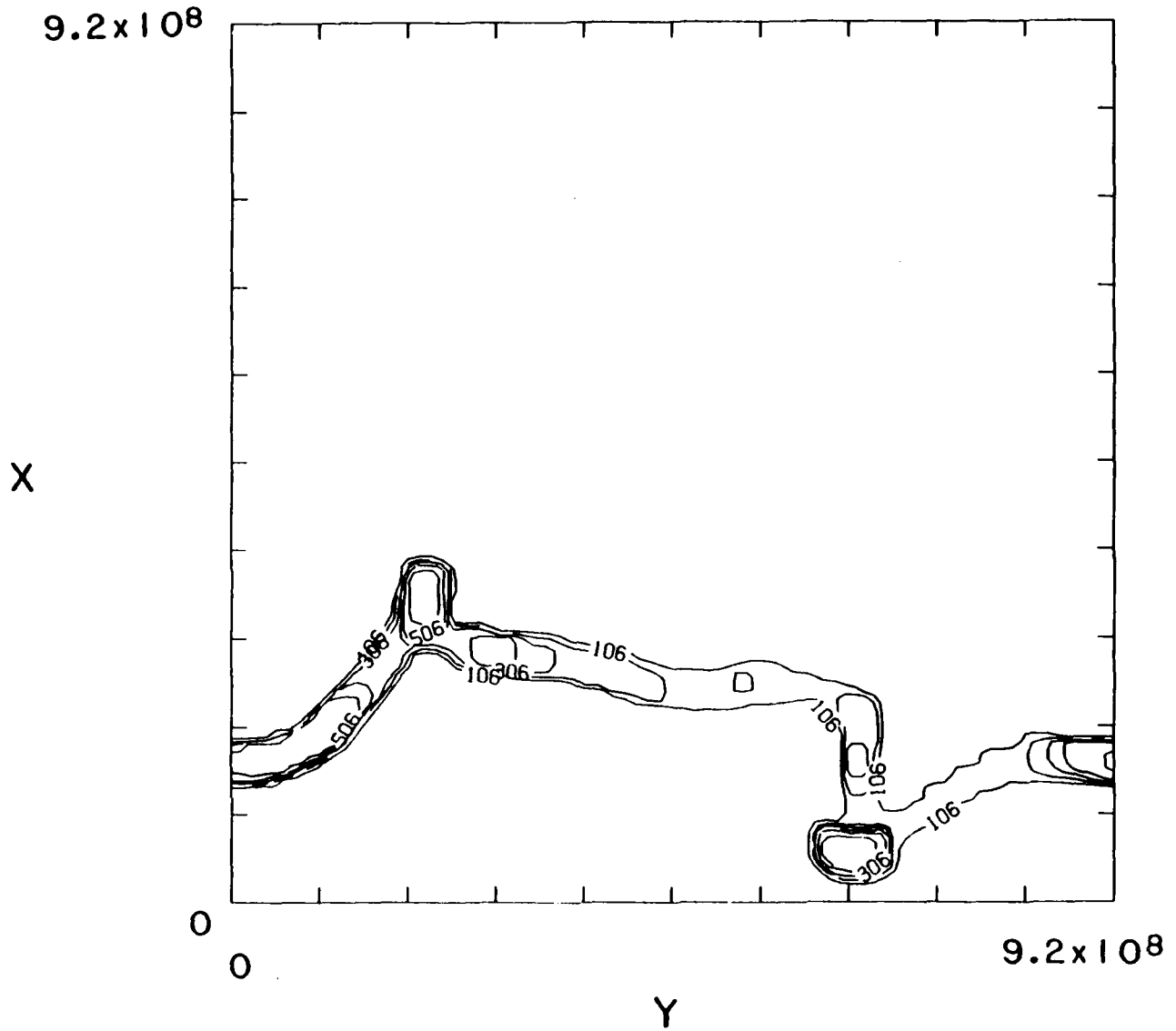

Figure 9. Contour plot of mass density at final time for two-dimensional simulation.

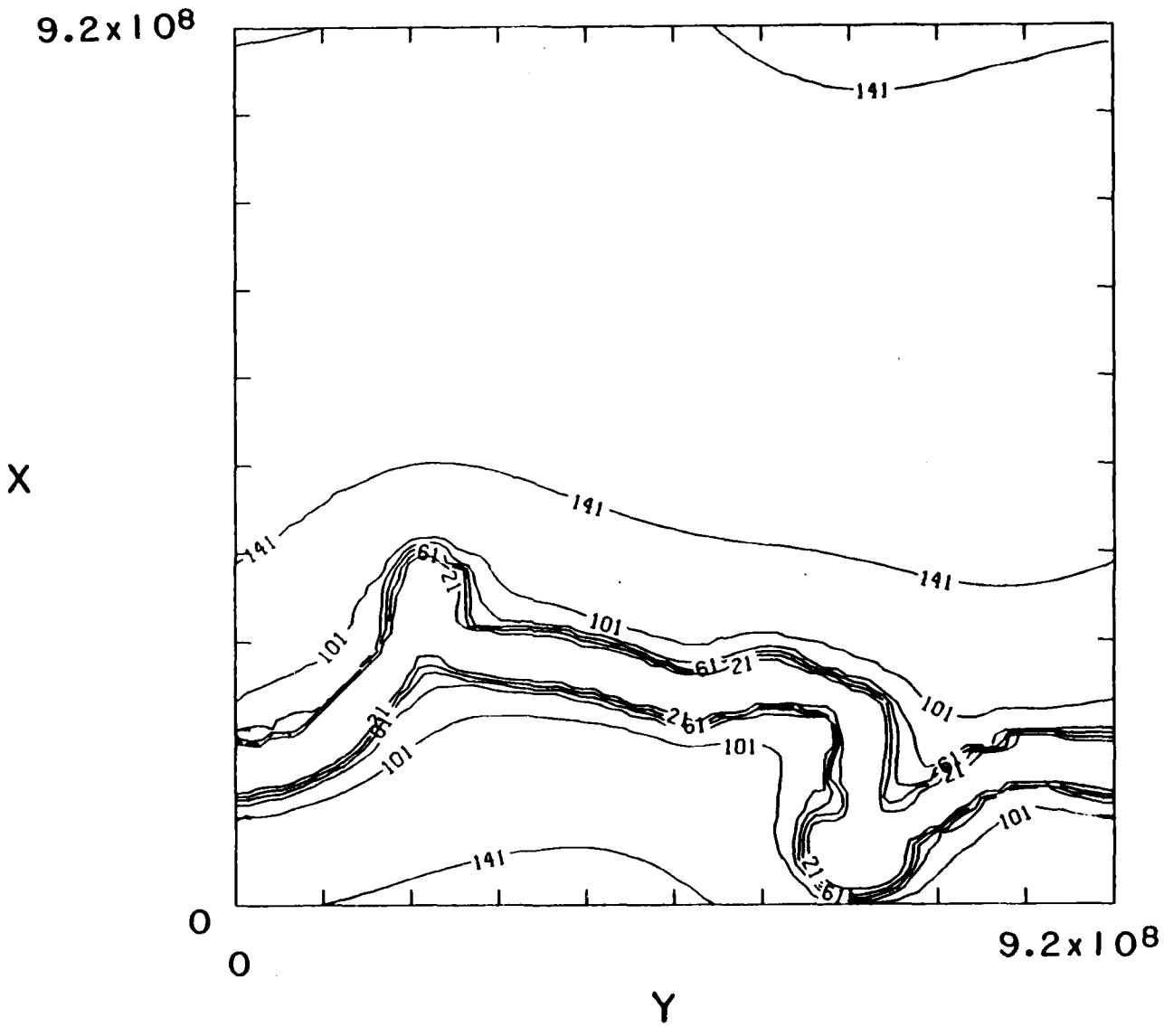

Figure 10. Contour plot of temperature at final time for two-dimensional simulation.

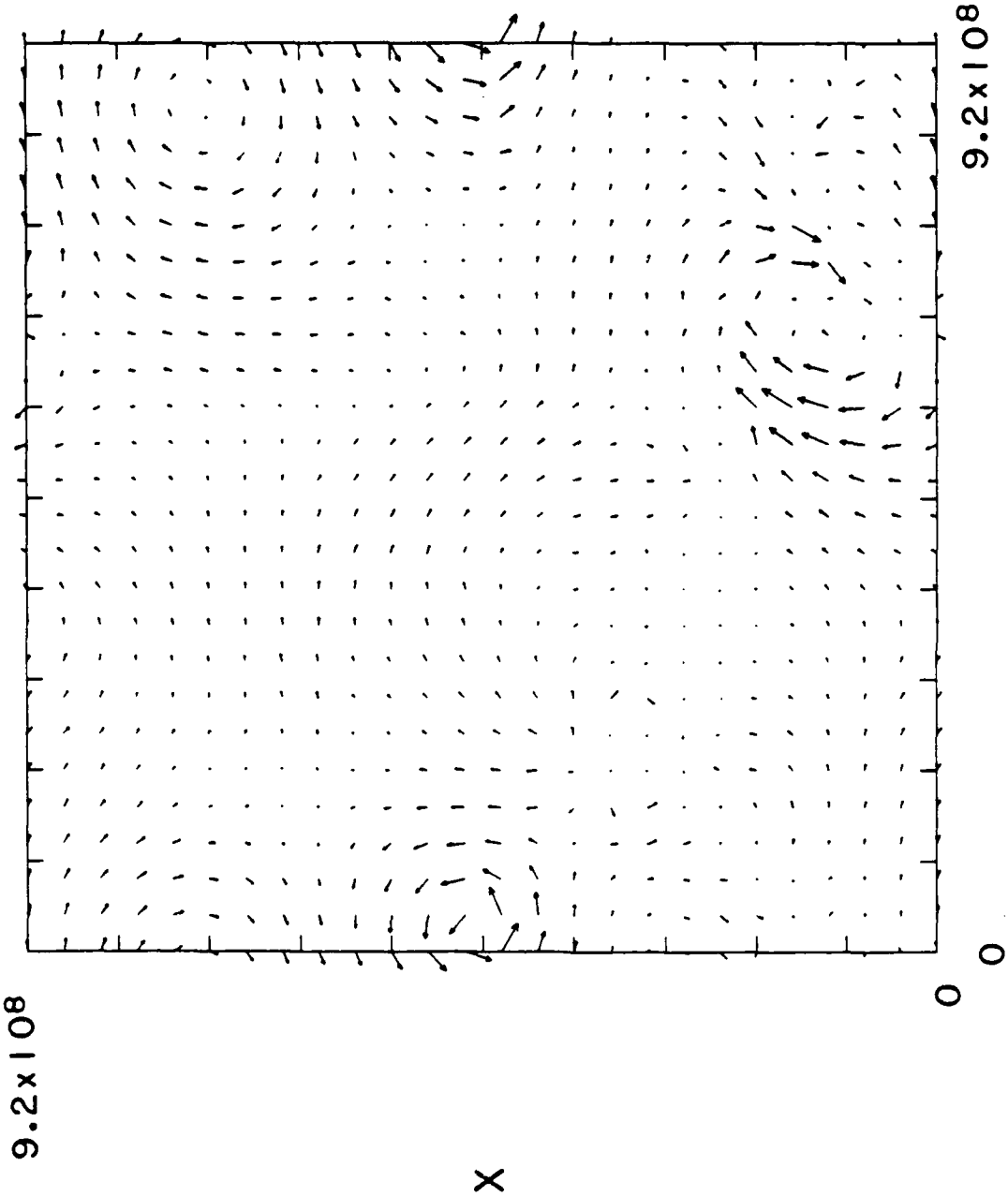

Figure 11. Vector plot of velocity field at final time for two-dimensional simulation.

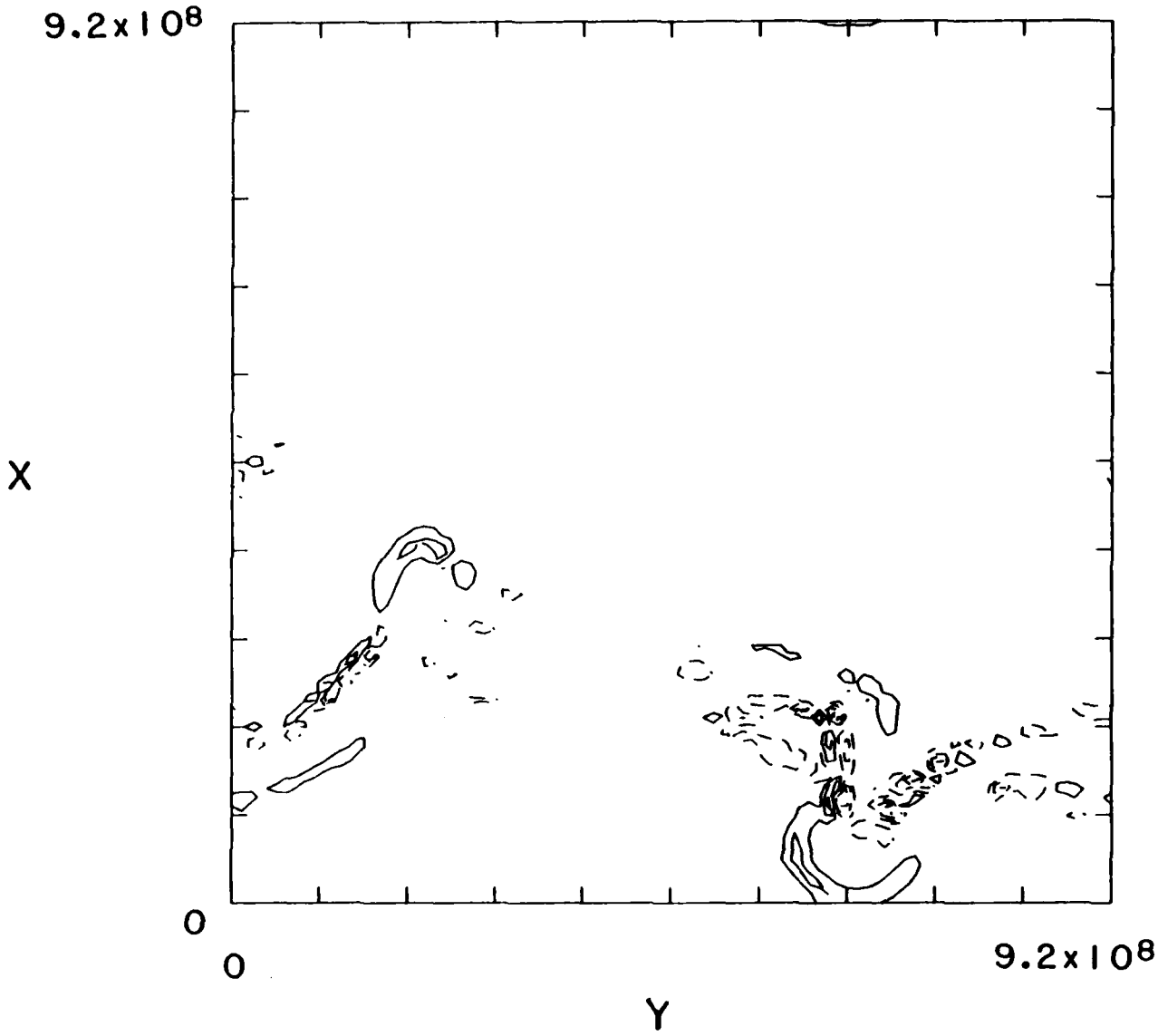

Figure 12. Contour plot of dilation factor at final time for two-dimensional simulation.

END

7-87

DTIC